Electron–heavy-nucleus bremsstrahlung at highly relativistic impact energies

D. H. Jakubassa-Amundsen
Mathematics Institute, University of Munich, Theresienstrasse 39, DE-80333 Munich, Germany
(Received 28 June 2010; published 22 October 2010)

Bremsstrahlung including the polarization correlations is revisited by presenting a theoretical model which is suited for the short-wavelength limit. The fast incoming electron is described by a Sommerfeld-Maue function, whereas for the outgoing electron an exact Dirac function is used. The cross section for electrons radiatively scattered from gold is calculated in the impact energy range 0.2–10 MeV and is compared to results from the Elwert-Haug theory and to available experimental data and relativistic partial-wave calculations. As an ultrarelativistic benchmark, the polarization correlations for 10 MeV electrons and 3–10 MeV photons are also given.

DOI: 10.1103/PhysRevA.82.042714 PACS number(s): 34.80.Pa, 41.60.−m

I. INTRODUCTION

With the recent experimental and theoretical investigation of radiative electron capture and radiative ionization by bare, heavy projectiles aiming at differential cross sections [1–3] and linear photon polarization [4–6], the interest in the bremsstrahlung process has been revived. The linear polarization P_1 of bremsstrahlung photons emitted from unpolarized high-energy electrons colliding with target atoms was extensively studied some 50 years ago (see, e.g., [7–13]). Also the spin asymmetry A from polarized electrons was measured and interpreted [14–19]. However, the predictions for the further polarization correlations which relate to linearly polarized photons, published by Tseng and Pratt [10] for the wide impact energy range from 5 keV to 1 MeV, have never been tested experimentally.

With the advent of novel-type Compton polarimeters, a series of experiments has been started to measure, for 100 keV electrons, the dependence of all these polarization correlations on photon energy and angle [20,21]. It is planned to extend the measurements to several MeV impact energy in the near future [22], which calls for theoretical predictions in this highly relativistic regime.

Two theoretical prescriptions have become standard for bremsstrahlung, both treating the photon field to first order. The first model, with results for the differential cross section and for P_1, dates back to Bethe, Olsen, and Maximon [7,23] in the ultrarelativistic regime, as well as to Elwert and Haug [9,24] for weakly relativistic collision systems. In this theory the electronic wave functions in the potential of a bare target nucleus of charge number Z are described by the Sommerfeld-Maue (SM) functions [25]. These functions reproduce the Coulomb wave functions in the nonrelativistic regime and approximate the exact Dirac functions for the higher energies. More precisely, they agree with the Dirac functions up to order $Z\alpha$ (where $\alpha = e^2/\hbar c$ is the fine structure constant), i.e., in the weak-relativistic regime. However, they become again exact in the ultrarelativistic regime, provided the distance r from the nucleus is much larger than $Z\alpha/p$ where p is the electron momentum [26]. Consistent with these two regions of applicability, a higher-order contribution to the transition matrix element is dropped such that the remaining radiation matrix element can be expressed in closed form. This is the advantage of the SM theory (which has become known as the Elwert-Haug theory). Based on this theory, Olsen and Maximon [7] have extracted a simple analytic formula for P_1 in the ultrarelativistic regime.

The second model differs from the first by using exact Dirac functions in place of the SM functions, with no further approximation. This necessitates a partial-wave representation of the differential cross section [8,27,28]. While SM results are available up to 15 MeV [9,24] and beyond 20 MeV impact energy [7], partial-wave results exist mostly at energies up to 2 MeV [10,29]. The reason is the strongly increasing numerical effort involved, since at higher energies the number of partial waves, needed for convergence, becomes very large. There are also a few results at 5 MeV and beyond [30,31], and even at the ultrarelativistic limit [32]. However, in these high-energy partial-wave calculations, the photon angle is not resolved.

Figure 1 gives an overview of existing results for the extrema of P_1 as a function of photon emission angle. The case is studied where the photon carries away 90% of the energy of the electron, which impinges on gold, while the scattered electron is not observed. Included are SM results covering the whole impact energy region under consideration. Both models agree fairly well with the available experimental data, showing that the two extrema merge and that P_1 remains finite (of order unity [7]) in the ultrarelativistic regime.

The fact that the polarization correlations related to linearly polarized photons are, with the exception of P_1, purely relativistic (since they vanish in the nonrelativistic limit and increase with $Z\alpha$ [10]) makes them a sensitive tool for studying the validity of the SM functions beyond the weak-relativistic regime. The judgment of the SM functions by a direct comparison between the SM theory and the partial-wave model is, however, hampered by two facts. First, there are *two* SM functions, often relating to very different energies, which enter into the transition matrix element, and second, the SM theory is subject to an additional approximation beyond replacing the Dirac functions by the SM functions.

Therefore we introduce a prescription, termed the Dirac-Sommerfeld-Maue (DSM) theory, where only *one* SM function, representing the fast (initial) electron, is introduced into the radiation matrix element. The outgoing electron, on the other hand, is described by an exact Dirac function. Such a hybrid theory where the initial and final wave functions are not eigenstates to the same Hamiltonian may suffer from nonorthogonality effects or from inconsistencies. In fact, orthogonality between the initial and final states holds only

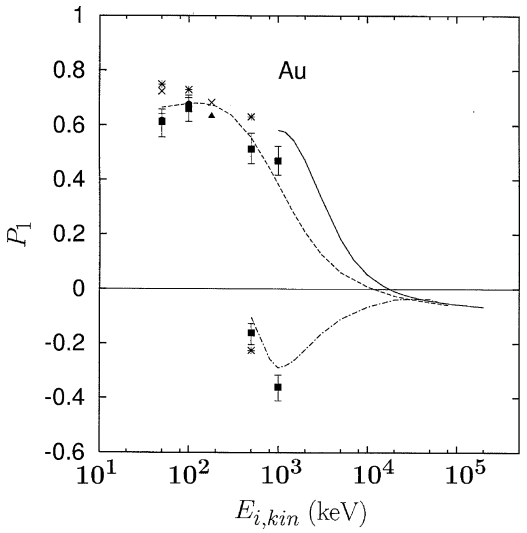

FIG. 1. Linear polarization P_1 of photons emitted with energy $\omega = 0.9E_{i,\mathrm{kin}}$ in e-Au collisions as a function of the collision energy $E_{i,\mathrm{kin}} = E_i - c^2$. For each $E_{i,\mathrm{kin}}$, the photon angle is chosen such that P_1 has its maximum value (upper points and curves) and its minimum value (occurring at larger angles; lower points and curves). The broken and chain curves are the present SM results for bare Au. The full line results from the analytic formula (7.1) with (6.23) of [7], valid in the forward regime only. The calculations of [8] ($\times$) and [10] ($*$) result from the partial-wave model. Experimental results (near the extrema of P_1) are taken from [11] (■), [12] (▲), [13] (●).

to first order in $Z\alpha$ (like in the SM theory) except in the ultrarelativistic limit.

Our argumentation in favor of the DSM approach is the following. There is a one-to-one correspondence between the SM functions and the nonrelativistic Coulomb waves, since the respective transformation operator, $e^{i\boldsymbol{k}_i\boldsymbol{r}}(1 - \frac{ic}{2E_i}\boldsymbol{\alpha}\cdot\boldsymbol{\nabla})\,e^{-i\boldsymbol{k}_i\boldsymbol{r}}$ [see Eq. (2.3) below] is invertible. Therefore, together with the bound states, the SM functions form a complete set and hence a basis for the expansion of a Dirac wave. Replacing the Dirac wave by an SM function of the same momentum is therefore equivalent to truncating this expansion after the first term. Hence the DSM model is, at high enough energy (i.e., when the difference between the two functions is small and the remaining terms of the expansion of minor importance), a consistent perturbative approach. Its great advantage as compared to the exact relativistic theory is the omission of a partial-wave expansion of the initial state, which at 10 MeV (and $Z > 40$) would require more than 120 partial waves for an accuracy of the differential cross section below 5% [31].

Only bare nuclei are considered in the present calculations. We will concentrate mostly on the short-wavelength limit (SWL), the tip of the bremsstrahlung spectrum where the whole collision energy is transferred to the photon, leaving the outgoing electron at the continuum threshold of the nucleus. Such an SWL collision system has several advantages. First, for high-Z targets, the slow outgoing electron, according to the criteria given above, can never be well described by an SM function, calling for an improvement beyond the SM model. Second, due to the large momentum transferred to the nucleus, regions of space close to the nucleus are selected which are the crucial ones for testing the validity of the SM function at high energy. Third, for sufficiently high impact energies, only a few partial waves of the final state are required [32,33], which makes the DSM calculations feasible beyond 2 MeV.

There exist some SM and partial-wave results at the SWL when Z is high. The SM calculations are done for the differential cross sections [24,31] and P_1 [9] up to 15 MeV. The partial-wave results also concern the differential cross sections [8,31,33,34] and P_1 [8,34] at energies mostly below 2 MeV. In [34–36] another noticeable advantage of the SWL was explored: the smooth transition between bremsstrahlung at threshold and radiative recombination (RR) of a free electron into infinitely high lying Rydberg states of the target. By extrapolating RR to the continuum threshold, partial-wave results up to 5 MeV can readily be obtained [37]. Such results, extended to the polarization correlations pertaining to doubly differential cross sections, were used in [38] to show that for heavy nuclei the electron energy has to exceed 5 MeV in order to describe all polarization correlations accurately with the help of SM functions.

In Sec. II, we formulate the DSM theory for the SWL and furnish the numerical details in Sec. III. Results for the doubly differential photon emission cross section (integrated over the electronic angular distribution) for 0.18–10 MeV electrons scattering from Au^{79+} are given in Sec. IV and are compared with the SM theory, the partial-wave model, and experiment. The relation between the differential cross sections for radiative recombination and bremsstrahlung at threshold is explored to extract additional partial-wave results. Finally, for 10 MeV electrons, results are presented for all polarization correlations relating to linearly polarized photons. There, the DSM theory is used at the SWL and the SM theory for the lower photon energies (Sec. V). Concluding remarks are given in Sec. VI. Atomic units ($\hbar = m = e = 1$) are used unless indicated otherwise.

II. THE DSM THEORY FOR BREMSSTRAHLUNG

We consider the scattering of a high-energy electron of (total) energy E_i and spin σ_i from a bare point nucleus of charge Z and allow for the simultaneous emission of a bremsstrahlung photon of energy ω. The doubly differential cross section for the emission of the photon into the solid angle $d\Omega_k$ is given by [28,39,40]

$$\frac{d^2\sigma}{d\omega\, d\Omega_k} = \frac{4\pi^2\omega k_f E_f}{c^3 v}\sum_{\sigma_f}\int d\Omega_f\, |[\boldsymbol{e}_\lambda\cdot\boldsymbol{W}_{\mathrm{rad}}(\sigma_f,\sigma_i)]|^2, \tag{2.1}$$

where v is the collision velocity. The energy $E_f = \sqrt{(k_f c)^2 + c^4}$ of the scattered electron is fixed by energy conservation, $E_f = E_i - \omega$. Assuming that the electron is not observed, we have summed over its final spin σ_f and integrated over the solid angle $d\Omega_f$ of emission.

To first order in the electron-photon interaction, the transition matrix element reads

$$\boldsymbol{e}_\lambda\cdot\boldsymbol{W}_{\mathrm{rad}}(\sigma_f,\sigma_i) = \int d\boldsymbol{r}\; \psi_f^{(\sigma_f)\dagger}(\boldsymbol{r})\,(\boldsymbol{\alpha}\cdot\boldsymbol{e}_\lambda)\,\psi_i^{(\sigma_i)}(\boldsymbol{r})\,e^{-i\boldsymbol{k}\boldsymbol{r}}. \tag{2.2}$$

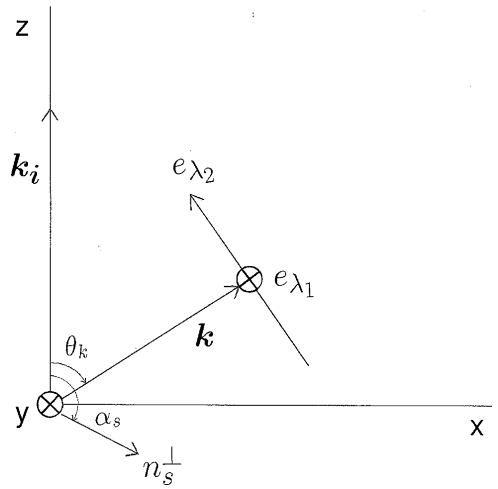

FIG. 2. Collision geometry. The y axis and $\boldsymbol{e}_{\lambda_1}$ point into the drawing plane (marked by the backside $\otimes$ of an arrow). $n_s^\perp$ is the projection of $\boldsymbol{n}_s$ onto the (x,z) plane.

Here, $\boldsymbol{\alpha} = (\alpha_x,\alpha_y,\alpha_z)$ is the vector of Dirac matrices, $\boldsymbol{e}_\lambda$ the polarization direction of the photon, and $\psi_i^{(\sigma_i)}$ and $\psi_f^{(\sigma_f)}$, respectively, the initial and final states of the electron.

The incoming electron is described by a Sommerfeld-Maue function [7,26]. Choosing the z axis along the momentum $\boldsymbol{k}_i$ of the incoming electron and employing spherical coordinates $\boldsymbol{r} = \{r,\vartheta,\varphi\}$, this function reads

$$\begin{aligned}\psi_i^{(\sigma_i)}(\boldsymbol{r}) &= N_{k_i} e^{ik_i r\cos\vartheta}\left\{ {}_1F_1(i\eta_i,1,ik_i r(1-\cos\vartheta)) + \frac{iZ}{2c}\right.\\ &\times\left[\alpha_z(\cos\vartheta-1)+\frac{1}{2}\alpha_-\sin\vartheta\, e^{i\varphi}+\frac{1}{2}\alpha_+\sin\vartheta\, e^{-i\varphi}\right]\\ &\left.\times\, {}_1F_1(1+i\eta_i,2,ik_i r(1-\cos\vartheta))\right\} u_{k_i}^{(\sigma_i)},\end{aligned} \tag{2.3}$$

where $\eta_i = ZE_i/k_i c^2$, $\alpha_\pm = \alpha_x \pm i\alpha_y$, N_{k_i} the normalization constant with the modulus $|N_{k_i}|^2 = \eta_i/[4\pi^2(1-e^{-2\pi\eta_i})]$, and ${}_1F_1$ a confluent hypergeometric function.

We choose a geometry (see Fig. 2) where the collision plane, which is spanned by $\boldsymbol{k}_i$ and the photon momentum $\boldsymbol{k} = k(\sin\theta_k,0,\cos\theta_k)$, coincides with the (x,z) plane. The plane perpendicular to $\boldsymbol{k}$ is spanned by the polarization vectors $\boldsymbol{e}_{\lambda_1} = (0,1,0)$ and $\boldsymbol{e}_{\lambda_2} = (-\cos\theta_k,0,\sin\theta_k)$, and an arbitrary electron spin direction is characterized by $\boldsymbol{n}_s = \{1,\alpha_s,\varphi_s\}$. Then a fixed photon polarization $\boldsymbol{e}_\lambda$ and electron plane-wave spinor $u_{k_i}^{(\sigma_i)}$ are represented in the following way [41]:

$$\begin{aligned}\boldsymbol{e}_\lambda &= \sin\varphi_\lambda \boldsymbol{e}_{\lambda_1} + \cos\varphi_\lambda \boldsymbol{e}_{\lambda_2},\quad \varphi_\lambda\in[0,\pi),\\ u_{k_i}^{(\sigma_i)} &= e^{-i\varphi_s/2}\cos\frac{\alpha_s}{2}u_{k_i}^{(+)} + e^{+i\varphi_s/2}\sin\frac{\alpha_s}{2}u_{k_i}^{(-)},\\ &\alpha_s,\varphi_s\in[0,2\pi),\end{aligned} \tag{2.4}$$

where $u_{k_i}^{(+)} = C_{k_i}(1,0,ck_i/(E_i+c^2),0)$ and $u_{k_i}^{(-)} = C_{k_i}(0,1,0,-ck_i/(E_i+c^2))$, with $C_{k_i} = [(E_i+c^2)/2E_i]^{1/2}$, are plane-wave four-spinors with electron spins parallel and, respectively, antiparallel to $\boldsymbol{k}_i$. For $\varphi_s = 0$, α_s describes spin rotation in the scattering plane.

For the outgoing electron, a Dirac continuum state is used, the partial-wave decomposition of which is given by [41]

$$\begin{aligned}\psi_f^{(\sigma_f)\dagger}(\boldsymbol{r}) &= \sum_{jlm}\left(w_{\sigma_f}^\dagger\, Y_{jlm}(\Omega_f)\right)\psi_{jlm}^\dagger(\boldsymbol{r})(-i)^l e^{i\delta_{lj}},\\ \psi_{jlm}(\boldsymbol{r}) &= \begin{pmatrix} g_{jl}(r)Y_{jlm}(\Omega)\\ if_{jl}(r)Y_{jl'm}(\Omega)\end{pmatrix},\end{aligned} \tag{2.5}$$

where Y_{jlm} is a vector spherical harmonic [42], $l' = l\pm 1$ for $j = l\pm\frac{1}{2}$, w_{σ_f} is a linear combination of the two-spinors $\chi_{\frac{1}{2}} = (1,0)$ and $\chi_{-\frac{1}{2}} = (0,1)$, and δ_{lj} is the phase shift.

Let us now restrict ourselves to outgoing electrons at the continuum threshold. When $k_f \to 0$, the radial functions have a simple representation in terms of Bessel functions J_ν [8,43],

$$\begin{aligned} f_{jl}(r) &= \frac{1}{r}\frac{\kappa}{|\kappa|}\frac{1}{c}\sqrt{\frac{Z}{k_f}}J_{2\gamma}(\sqrt{8Zr}),\\ g_{jl}(r) &= -\frac{1}{r}\frac{\kappa}{|\kappa|}\frac{1}{\sqrt{k_f Z}}\\ &\times[\sqrt{2Zr}J_{2\gamma-1}(\sqrt{8Zr}) - (\gamma+\kappa)J_{2\gamma}(\sqrt{8Zr})],\\ \gamma &= \sqrt{\kappa^2-(Z/c)^2},\quad \kappa = \begin{cases}-(l+1), & j = l+\frac{1}{2},\\ l, & j = l-\frac{1}{2}.\end{cases}\end{aligned} \tag{2.6}$$

In the following, we make use of the representation of the vector spherical harmonics [42],

$$\begin{aligned} Y_{jlm}(\Omega_f) &= \sum_{\mu,m_s} Y_{l\mu}(\Omega_f)\chi_{m_s}\left(l\mu\tfrac{1}{2}m_s\,|\,jm\right),\\ &|\mu|\leqslant l,\quad m_s = \pm\frac{1}{2},\end{aligned} \tag{2.7}$$

where we have introduced the Clebsch-Gordan coefficients $(l\mu\frac{1}{2}m_s|jm)$. Further we apply the orthogonality property of the spherical harmonics Y_{lm} and the Clebsch-Gordan coefficients, as well as the completeness relation $\sum_{\sigma_f} w_{\sigma_f} w_{\sigma_f}^\dagger = 1$. Then, inserting (2.5) into the radiation matrix element (2.2) and performing the integration over Ω_f and the summation over σ_f in (2.1), the doubly differential cross section reduces to an incoherent sum over the final-state partial-wave contributions,

$$\frac{d^2\sigma}{d\omega\, d\Omega_k} = \frac{4\pi^2\omega k_f E_f}{c^3 v}\sum_{jlm}|M_{jlm}|^2, \tag{2.8}$$

$$\begin{aligned} M_{jlm} &= \int d\boldsymbol{r}\,\psi_{jlm}^\dagger(\boldsymbol{r})(\boldsymbol{\alpha}\cdot\boldsymbol{e}_\lambda)\psi_i^{(\sigma_i)}(\boldsymbol{r})\\ &\times e^{-ikr(\cos\vartheta\cos\theta_k+\sin\vartheta\sin\theta_k\cos\varphi)}.\end{aligned}$$

III. NUMERICAL DETAILS

Since $\psi_f^{(\sigma_f)}$ is a threshold continuum state, its angular dependence is rather weak. Therefore we have restricted ourselves to including only the $j = \frac{1}{2}$ and $j = \frac{3}{2}$ states in the partial-wave expansion. For $Z = 79$ and impact energies of 2 MeV and above, even the d-wave contribution ($j = \frac{3}{2}, l = 2$)

is reduced by several orders of magnitude (except in a narrow forward cone) so that one might even restrict oneself to the s and p waves at the higher collision energies (see also [33]).

Let us split M_{jlm} into the two contributions from the upper and lower components of ψ_{jlm},

$$M_{jlm} = \sum_{m_s=\pm\frac{1}{2}} \begin{pmatrix} \chi_{m_s} \\ 0 \end{pmatrix}^\dagger \left(l \;\; m - m_s \frac{1}{2} m_s \mid jm \right) \times \int d\boldsymbol{r}\, g_{jl}(r) Y^*_{l,m-m_s}(\Omega) \phi_{\lambda i}(\boldsymbol{r}) - i \sum_{m_s=\pm\frac{1}{2}} \begin{pmatrix} 0 \\ \chi_{m_s} \end{pmatrix}^\dagger \times \left(l' m - m_s \frac{1}{2} m_s \mid jm \right) \int d\boldsymbol{r}\, f_{jl}(r) Y^*_{l',m-m_s}(\Omega) \phi_{\lambda i}(\boldsymbol{r}), \tag{3.1}$$

where $\phi_{\lambda i}$ abbreviates the (four-spinor) part of the integrand in M_{jlm} which multiplies $\psi^\dagger_{jlm}(\boldsymbol{r})$.

With the representation of $Y_{l\mu}$ in terms of the Legendre functions P_l^μ (see [42] and Sec. 8.7 of [44]),

$$Y_{l\mu}(\Omega) = \sqrt{\frac{2l+1}{4\pi}} \sqrt{\frac{(l-\mu)!}{(l+\mu)!}} P_l^\mu(\cos\vartheta) e^{i\mu\varphi}, \tag{3.2}$$

the φ integral of the spatial integrals in (3.1) can be done analytically,

$$\int_0^{2\pi} d\varphi e^{-i\mu\varphi} e^{-iq_\perp r \sin\vartheta \cos\varphi} e^{is\varphi} = 2\pi (-i)^{|\mu-s|} J_{|\mu-s|}(q_\perp r \sin\vartheta). \tag{3.3}$$

Here we have introduced the transverse momentum transfer $q_\perp = k \sin\theta_k$, and $s \in \{0, 1, -1\}$ from the contribution of $\psi_i^{(\sigma_i)}(\boldsymbol{r})$. Thus the double integrals to be performed numerically are, for example,

$$\int_0^\infty dr\, r^{3/2} J_{2\gamma-1}(\sqrt{8Zr}) \int_{-1}^1 d(\cos\vartheta) P_l^\mu(\cos\vartheta) \times J_{|\mu-s|}(q_\perp r \sin\vartheta) e^{iq_z r\cos\vartheta} {}_1F_1\big(i\eta_i, 1, ik_i r(1-\cos\vartheta)\big), \tag{3.4}$$

where we have introduced the longitudinal momentum transfer, $q_z = k_i - k\cos\theta_k$. The other integrals which occur are related to (3.4) by replacing $J_{2\gamma-1}(\sqrt{8Zr})$ by $r^{-1/2} J_{2\gamma}(\sqrt{8Zr})$ or by replacing the confluent hypergeometric function by $h(\vartheta)\, {}_1F_1\big(1 + i\eta_i, 2, ik_i r(1-\cos\vartheta)\big)$ with $h(\vartheta) \in \{1, \cos\vartheta, \sin\vartheta\}$, and which are of better convergence than (3.4).

For the treatment of radial integrals involving Bessel functions (which are weakly decaying, but strongly oscillating), we make use of the fact that integrals of the type $\int_1^\infty dr\, r^\mu J_\nu(r)$ are convergent for any $\nu \in \mathbb{R}, \mu \in \mathbb{C}$; see example 144 in [45]. This can be shown either by using complex analysis (see, e.g., [46] for a related integral) or, for the case $\mu + \nu > -1$, by introducing convergence generating functions and considering the limit as they tend to unity (see pp. 711 and 684 in [44]),

$$\lim_{\epsilon\to 0} \int_0^\infty dr r^\mu J_\nu(ar) e^{-\epsilon r} = \frac{2^\mu}{a^{\mu+1}} \frac{\Gamma\left(\frac{\nu+\mu+1}{2}\right)}{\Gamma\left(\frac{\nu-\mu+1}{2}\right)}, \quad a > 0. \tag{3.5}$$

Using the fact that the angular integral in (3.4) is a smooth function of r, we can apply the above technique by considering, in place of (3.4), a sequence of integrals,

$$I_\epsilon = \int_0^{r_{\max}(\epsilon)} dr\, F(r) e^{-\epsilon r}, \tag{3.6}$$

where F denotes the r integrand in (3.4) after having performed the angular integral, and $r_{\max}(\epsilon) \sim 8/\epsilon$ is an upper cutoff large enough to ensure convergence of the integral for fixed ϵ. The appropriate choice of ϵ is dictated by the momentum transfer to the nucleus, $q = (q_\perp^2 + q_z^2)^{1/2} = |\boldsymbol{k}_i - \boldsymbol{k}|$, and the nuclear charge Z. It increases (linearly) with Z and also with q (respectively, with photon angle and impact energy). This behavior is based on the fact that rapid oscillations of the angular-dependent functions (when q is large) lead to a reduction of the radiation matrix element and to convergence at comparatively small r. This convergence is also speeded up when the Bessel function $J_\nu(\sqrt{8Zr})$ changes sign more rapidly (i.e., when Z is large). From this numerics we estimate the accuracy of the differential cross section and P_1 to be about 1%, while the other polarization correlations are less accurate, particularly at the backward photon angles for high impact energies (5%–10%). Further inaccuracies, predominantly at very small angles, are introduced by terminating the final-state partial-wave series at $j = \frac{3}{2}$. For angles $\theta_k \lesssim 10^\circ$ they amount to 10%–15% when $E_{i,\mathrm{kin}} \sim$ 200–400 keV, dropping to $\lesssim$5% at 2 MeV.

IV. CROSS SECTION RESULTS

We start by providing the relation between radiative recombination and bremsstrahlung at threshold. As shown in [34] this relation invokes the density of states, dn/dE, where n is the main quantum number of the Rydberg state and E the energy. The derivation given below pertains to the experimental treatment of cusp phenomena, but involves strictly the limit $n \to \infty$. For simplicity we consider the nonrelativistic one-electron case. The nonrelativistic theory for bremsstrahlung emission at the SWL ($\omega = \frac{1}{2} v^2$) gives the following formula for the doubly differential cross section (see Chap. 92 in [26]), assuming only dipole radiation,

$$\frac{d^2\sigma^{\mathrm{SWL}}}{d\omega\, d\Omega_k} = 16 Z^3 \frac{1}{c^3 v^5} \sin^2\theta_k. \tag{4.1}$$

On the other hand, the differential cross section for the radiative capture of a fast electron into a high Rydberg state of a bare nucleus can be written in the following way [47]:

$$\frac{d\sigma^{(n)}}{d\Omega_k} = \frac{(2\pi)^2 v}{c^3} \omega_n \varrho_n(v) \sin^2\theta_k. \tag{4.2}$$

In this expression, $\omega_n = \frac{1}{2} v^2 + \frac{Z^2}{2n^2}$ is the sum of the collision energy and the binding energy of the Rydberg state. ϱ_n is the electron momentum density, summed over the subshells corresponding to the state n,

$$\varrho_n(v) = \sum_{l=0}^{n-1} \sum_{m=-l}^{l} |\hat{\psi}_{nlm}(\boldsymbol{v})|^2 = \frac{8Z^5}{\pi^2 n^3} \frac{1}{(v^2 + Z^2/n^2)^4}, \tag{4.3}$$

which decreases with n according to n^{-3} for high n. However, in an experimental situation, one averages over the resolution $\Delta\omega$ of the photon detector. In particular, at the SWL, all

Rydberg states with $n \geqslant n_0$, where n_0 is given by $\Delta\omega = \omega_{n_0} - \frac{1}{2}v^2 = \frac{Z^2}{2n_0^2}$, cannot be resolved (see, e.g., [48] for the radiation from quasifree electrons). Therefore the measured quantity is

$$\left\langle \frac{d\sigma^{\mathrm{RR}}}{d\Omega_k} \right\rangle_{\Delta\omega} = \frac{1}{\Delta\omega} \sum_{n=n_0}^{\infty} \frac{d\sigma^{(n)}}{d\Omega_k}. \tag{4.4}$$

Now we claim that in the limit $\Delta\omega \to 0$, corresponding to $n_0 \to \infty$, the bremsstrahlung formula (4.1) is retrieved. By using the integral test for convergence [49], we find

$$\lim_{n_0\to\infty} n_0^2 \sum_{n=n_0}^{\infty} \frac{1}{n^3} = \frac{1}{2}. \tag{4.5}$$

Therefore,

$$\begin{aligned} &\lim_{n_0\to\infty} \left\langle \frac{d\sigma^{\mathrm{RR}}}{d\Omega_k} \right\rangle_{\Delta\omega} \\ &\quad = \lim_{n_0\to\infty} \frac{2n_0^2}{Z^2} \sum_{n=n_0}^{\infty} \frac{16}{n^3} \frac{Z^5 v}{c^3} \frac{1}{(v^2 + Z^2/n^2)^3} \sin^2\theta_k \\ &\quad = \frac{16Z^3}{c^3 v^5} \sin^2\theta_k = \frac{d^2\sigma^{\mathrm{SWL}}}{d\omega\, d\Omega_k}. \end{aligned} \tag{4.6}$$

Numerically, the RR cross sections $d\sigma^{(n)}/d\Omega_k$ are calculated for a series of n (typically up to $n \sim 16$) and are subsequently fitted by a power law $A_1(\theta_k)/n^3$ that is obeyed to high accuracy beyond $n \approx 8$ [37]. From the result (4.6) it follows that $d^2\sigma^{\mathrm{SWL}}/d\omega\, d\Omega_k = A_1(\theta_k)/Z^2$. Since the formula $Z^2/(2n^2)$ for the binding energy of high Rydberg states remains valid for heavy nuclei, this prescription can also be used in the relativistic case. (In Fig. 4 below, the additional factor $10^3/27.21$ is included to convert atomic units into keV.)

Figure 3 shows the angular dependence of the emitted photons for the two cases $E_{i,\mathrm{kin}} = 180$ and 380 keV. Comparison is made between the partial-wave model, the DSM theory, the SM theory, and experiment. It is seen that the SM cross sections are generally a factor of 2–3 too low (a fact well known from previous investigations [24,33] for high nuclear charge), the discrepancy increasing at the backward angles. As expected, the partial-wave theory describes the experiment nicely, but this is also true for the DSM model at angles $\theta_k \lesssim 120^\circ$. At the larger emission angles, relativity plays a more and more important role (due to the increasing momentum transfer) such that the SM functions are no longer appropriate. Turning to the importance of screening (the partial-wave calculations are done for the neutral target as used in experiment, while the SM and DSM results are for a bare nucleus), we note that for $E_{i,\mathrm{kin}} \gtrsim 200$ keV the relevant electron-nucleus distances at the SWL (given by the inverse momentum transfer) lie within the K-shell radius, even in the forward hemisphere. Thus screening affects the normalization rather than the shape of the wave function [33]. In the angular regime pertaining to the total cross section, screening amounts to 5%–10% at impact energies between 100 keV and 1 MeV [31,33], being small at the backward angles and decreasing with energy [10,24,28]. So screening is at most of the same order as the numerical accuracy of the DSM results, which justifies its neglect for all cases considered.

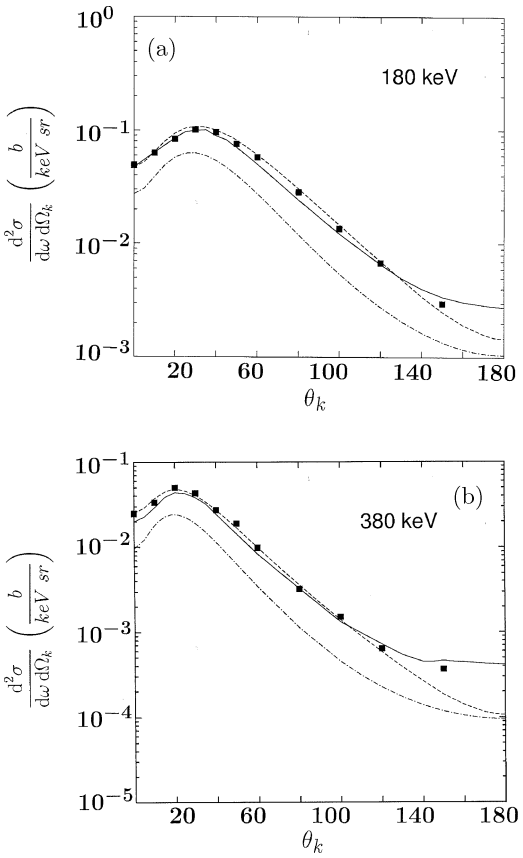

FIG. 3. Doubly differential cross section for photon emission from collisions of (a) 180 keV and (b) 380 keV electrons with Au at the SWL ($\omega = 180$ and 380 keV, respectively) as a function of photon angle θ_k. Shown are the results from the partial-wave model [8] (solid curve), DSM theory (dashed curve), SM theory (dot-dashed curve), and experiment [50] (squares).

When the impact energy is further increased, the cross section drops rapidly for $\theta_k \gtrsim 20^\circ$ without much changing its overall shape. However, the photons are more and more focused at very small angles, which even leads to an increase of the cross section at $\theta_k = 0$ for $E_{i,\mathrm{kin}} \gtrsim 2$ MeV (Fig. 4). This behavior can be related to the dominant phase factor, $e^{i(\boldsymbol{k}_i - \boldsymbol{k})\boldsymbol{r}}$, in the radiation matrix element (2.2). We have $k_i c = \sqrt{E_i^2 - c^4}$ and in the SWL, $kc = \omega = E_i - c^2$ such that $k/k_i \to 1$ and $k_i - k \to c$ for $E_i \to \infty$ [33]. Therefore, at $\theta_k = 0$, the phase $(k_i - k)r\cos\vartheta$ tends to a constant (in k_i) with increasing E_i [at 2 MeV, $(k_i - k)/c = 0.9$]. Together with the prefactor ω in (2.1), this leads to an increase of the cross section. However, for any small but finite θ_k there exists some energy E_θ such that for $E_i > E_\theta$, $|\boldsymbol{k}_i - \boldsymbol{k}|$ increases strongly (eventually to ∞), leading to a steep decrease of the cross section with energy.

Concerning the validity of the DSM theory, we recall that the SM functions approach the exact functions for sufficiently large energies E_i, provided $r \gg Z\alpha/k_i$. For $\theta_k = 0$, this condition can be translated into

$$r \sim \frac{1}{|(k_i - k)\cos\vartheta|} \geqslant \frac{1}{(k_i - k)} \overset{!}{\gg} \frac{Z\alpha}{k_i}. \tag{4.7}$$

For $E_{i,\mathrm{kin}} = 2$, 5, and 10 MeV, the ratio $\frac{k_i}{k_i - k}$ is equal to, respectively, 5.4, 11.3, and 21.1. Thus for Au ($Z\alpha \approx 0.6$),

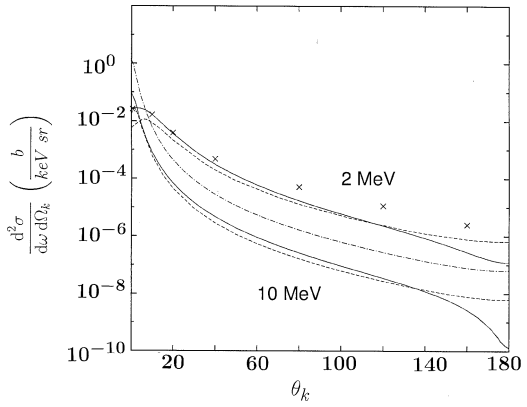

FIG. 4. Doubly differential cross section for photon emission from collisions of 2 MeV (upper curves) and 10 MeV (lower curves) electrons with Au^{79+} at the SWL as a function of photon angle θ_k. DSM model (solid curve), SM results (dashed curve). Included is the SM result for $E_{i,\mathrm{kin}} = 10$ MeV, $\omega = 5$ MeV (dot-dashed curve), as well as partial-wave results at 2 MeV (×) [37].

the SM initial-state function is reliable near and above 2 MeV at small angles (see also Fig. 4).

In the backward regime, on the other hand, say $\theta_k = 180^\circ$, the condition (4.7) has to be replaced by $(k_i + k)\,|\cos\vartheta| \ll k_i$. This holds only for polar angles close to 90° and therefore the DSM model performs worse. From Fig. 4 it follows that at 2 MeV there are still considerable deviations between the DSM and the partial-wave results for θ_k beyond 60°. As concerns the SM results, the inadequacy of the approximate final threshold state (irrespective of E_i) prevents a better agreement with the DSM model when the collision energy is increased.

In order to estimate the correction effects concerning nonorthogonality, we calculated the singly differential cross section $S_\omega \equiv d\sigma/dE_f (= d\sigma/d\omega)$ by integrating over the photon solid angle, and compared it to the respective cross section (termed S_1) when the transition operator is set to unity (i.e., in the absence of photons). For the Au target, the ratio S_1/S_ω is given by 0.0092 (for 180 keV), 0.0024 (for 380 keV), 3.5×10^{-5} (for 2 MeV), and 1.2×10^{-6} (for 5 MeV). Thus the correction from the overlap between the initial- and final-state wave functions is below the numerical accuracy of our calculations and can be neglected.

Included in Fig. 4 is the SM theory for photons carrying away only half the electron's energy ($\omega = E_{f,\mathrm{kin}} = 5$ MeV, where SM functions are appropriate except possibly at the largest angles). As compared to the SWL at 10 MeV, the corresponding cross section is enhanced at all angles and also shows the steep increase toward $\theta_k = 0$, while depending only weakly on the angle beyond 140°.

V. POLARIZATION CORRELATIONS

The polarization correlations for bremsstrahlung are specified in detail by Tseng and Pratt [10] using, however, a reference frame in which the z axis is aligned with the photon momentum rather than with the collision velocity. The starting point is the representation of the differential cross section (2.1) in the following form, making use of the time-reversal invariance [10]:

$$d\sigma = \tfrac{1}{2} d\sigma_0 (1 + C_{03}\xi_3 + C_{11}\zeta_1\xi_1 + C_{12}\zeta_1\xi_2 + C_{20}\zeta_2 + C_{23}\zeta_2\xi_3 + C_{31}\zeta_3\xi_1 + C_{32}\zeta_3\xi_2), \tag{5.1}$$

where ξ_k and ζ_k, $k = 1,2,3$, denote, respectively, the parameters for photon and electron (initial-state) polarization, and $d\sigma_0$ is the differential cross section averaged over the initial spin of the electron and summed over the final electron spin and photon polarization. C_{ik}, $i,k \in \{0,1,2,3\}$ are the nonvanishing correlation parameters. With $\boldsymbol{e}_\lambda$ from (2.4) for linear photon polarization, we have

$$\xi_1 = 2\sin\varphi_\lambda \cos\varphi_\lambda, \quad \xi_2 = 0, \quad \xi_3 = 1 - 2\sin^2\varphi_\lambda, \tag{5.2}$$

hence C_{12} and C_{32} do not occur. The electron spin direction $\boldsymbol{n}_s = (\zeta_1,\zeta_2,\zeta_3)$ is here defined with respect to the basis $\boldsymbol{\zeta}_1 = \boldsymbol{e}_x, \boldsymbol{\zeta}_2 = -\boldsymbol{e}_y, \boldsymbol{\zeta}_3 = -\boldsymbol{e}_z$ in our coordinate system (i.e., $\boldsymbol{\zeta}_3$ antiparallel to $\boldsymbol{k}_i$, $\boldsymbol{\zeta}_2$ aligned with $\boldsymbol{k} \times \boldsymbol{k}_i$, $\boldsymbol{\zeta}_1$ aligned with $\boldsymbol{k}_i \times \boldsymbol{\zeta}_2$).

The Stokes parameters P_1 and P_2 are obtained from the geometry where the spin direction $\boldsymbol{n}_s$ lies in the scattering plane [$\varphi_s = 0$ in (2.4), respectively, $\zeta_2 = 0$ in the above basis]. In that case, (5.1) reduces to $d\sigma = \frac{1}{2} d\sigma_0 (1 + C_{03}\xi_3 + C_{11}\zeta_1\xi_1 + C_{31}\zeta_3\xi_1)$. If we choose $\varphi_\lambda \in \{0, \frac{\pi}{2}\}$ then ξ_1 vanishes while $\xi_3 \in \{1, -1\}$. Thus we get

$$P_1 \equiv C_{03} = \frac{d\sigma(\varphi_\lambda = 0) - d\sigma(\varphi_\lambda = 90^\circ)}{d\sigma(\varphi_\lambda = 0) + d\sigma(\varphi_\lambda = 90^\circ)} = \frac{d\sigma(\boldsymbol{e}_{\lambda_2}) - d\sigma(\boldsymbol{e}_{\lambda_1})}{d\sigma(\boldsymbol{e}_{\lambda_2}) + d\sigma(\boldsymbol{e}_{\lambda_1})}. \tag{5.3}$$

P_1 is independent of ζ_1 and ζ_3 (respectively, of α_s, the polar angle of $\boldsymbol{n}_s$), such that also for unpolarized electrons, P_1 is calculated from (5.3).

For obtaining P_2 (respectively, C_{11} and C_{31}) we have to get rid of C_{03}, so we take $\varphi_\lambda \in \{45^\circ, 135^\circ\}$ where ξ_3 vanishes. P_2 is defined by

$$P_2(\alpha_s) = \frac{d\sigma(\varphi_\lambda = 45^\circ) - d\sigma(\varphi_\lambda = 135^\circ)}{d\sigma(\varphi_\lambda = 45^\circ) + d\sigma(\varphi_\lambda = 135^\circ)} = C_{11}\zeta_1 + C_{31}\zeta_3. \tag{5.4}$$

In contrast to P_1, P_2 does depend on α_s. It obeys the symmetry property $P_2(\alpha_s + \pi) = -P_2(\alpha_s)$ since the augmentation of α_s by π changes the sign of $\boldsymbol{n}_s$ (and hence of ζ_1 and ζ_3).

The polarization correlation C_{11} results from (5.4) by choosing $\boldsymbol{n}_s = \boldsymbol{\zeta}_1$ and noting that $\alpha_s = \frac{\pi}{2}$ corresponds to $\zeta_1 = 1$. In a similar way, setting $\boldsymbol{n}_s = \boldsymbol{\zeta}_3$ (with $\alpha_s = 0$ relating to $\zeta_3 = -1$), C_{31} is obtained. Explicitly,

$$P_{2\perp} \equiv P_2(90^\circ) = C_{11}, \qquad P_{2\parallel} \equiv P_2(0) = -C_{31}. \tag{5.5}$$

The remaining polarization correlations, C_{20} and C_{23}, characterize the electron spin polarization perpendicular to the scattering plane with $\zeta_1 = \zeta_3 = 0$, corresponding to $\alpha_s = \frac{\pi}{2}$.

Then one gets from (5.1), $d\sigma = \frac{1}{2} d\sigma_0 (1 + C_{03}\xi_3 + C_{20}\zeta_2 + C_{23}\zeta_2\xi_3)$. In order to eliminate C_{03} we sum over the photon polarization, i.e., we add the differential cross sections obtained from $\varphi_\lambda = 0\,(\xi_3 = 1)$ and from $\varphi_\lambda = \frac{\pi}{2}$

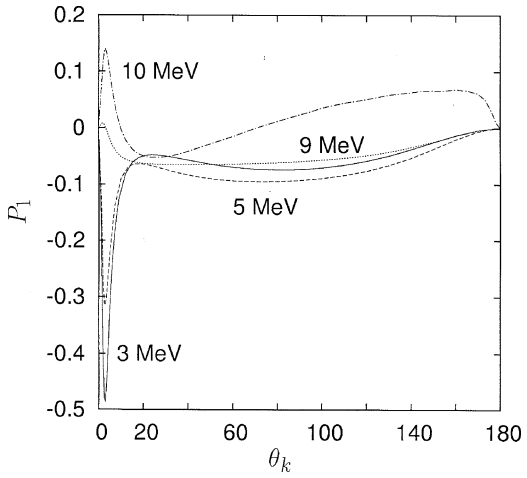

FIG. 5. Angular dependence of the linear photon polarization P_1 from 10 MeV electrons colliding with Au^{79+}. Shown are SM results for photon energies $\omega = 3$ MeV (solid curve), 5 MeV (dashed curve), and 9 MeV (dotted curve) as well as results from the DSM theory at the SWL (dot-dashed curve).

($\xi_3 = -1$). This leads to $\sum_\lambda d\sigma = d\sigma_0(1 + C_{20}\zeta_2)$. Consequently, representing $\boldsymbol{n}_s = \boldsymbol{\zeta}_2$ by $\varphi_s = -\frac{\pi}{2}$ and $\boldsymbol{n}_s = -\boldsymbol{\zeta}_2$ by $\varphi_s = \frac{\pi}{2}$, the spin asymmetry is calculated from

$$A \equiv C_{20} = \frac{\sum_\lambda [d\sigma(\uparrow) - d\sigma(\downarrow)]}{\sum_\lambda [d\sigma(\uparrow) + d\sigma(\downarrow)]}, \tag{5.6}$$

where $\uparrow$ and $\downarrow$ represent, respectively, the pairs $(\alpha_s,\varphi_s) = (\frac{\pi}{2}, -\frac{\pi}{2})$ and $(\frac{\pi}{2},\frac{\pi}{2})$.

The last correlation parameter, C_{23}, is not directly accessible. Let us define, for each spin direction, the linear polarization according to formula (5.3),

$$\begin{aligned} P_1(\uparrow) &= \frac{d\sigma_{\varphi_\lambda=0}(\uparrow) - d\sigma_{\varphi_\lambda=90^\circ}(\uparrow)}{d\sigma_0} = C_{03} + C_{23}, \\ P_1(\downarrow) &= \frac{d\sigma_{\varphi_\lambda=0}(\downarrow) - d\sigma_{\varphi_\lambda=90^\circ}(\downarrow)}{d\sigma_0} = C_{03} - C_{23}, \end{aligned} \tag{5.7}$$

with $d\sigma_0 = \frac{1}{2}\sum_\lambda [d\sigma(\uparrow) + d\sigma(\downarrow)]$. This leads to

$$C_{23} = \tfrac{1}{2}[P_1(\uparrow) - P_1(\downarrow)]. \tag{5.8}$$

Figure 5 shows the Stokes parameter P_1 for an impact energy of 10 MeV and photon energies between 3 and 10 MeV. From the investigation of [38], it follows that for P_1, the SM functions provide a satisfactory description if the kinetic energy is above 2 MeV, such that the application of the SM theory is basically justified. Away from the short-wavelength limit and for photon angles above 20° the linear polarization is negative (which means that the photons are predominantly polarized perpendicular to the collision plane, a purely relativistic effect) and varies only weakly with θ_k. However, there is a considerable overall rise of P_1 when ω is increased from 9 to 10 MeV. At very small angles, P_1 varies strongly with ω, showing a large negative peak for $\omega \lesssim \frac{1}{2}E_{i,\mathrm{kin}}$, but a positive peak when the SWL is approached. The change of the forward maximum of P_1 to a minimum when ω is decreased was also found at lower impact energies (see Fig. 10 of Ref. [10] for $E_{i,\mathrm{kin}} = 0.5$ MeV). In the high-energy regime, the forward maximum decreases with impact energy at the SWL; for $\omega = 0.9\,E_{i,\mathrm{kin}}$, even to a negative value (see Fig. 1).

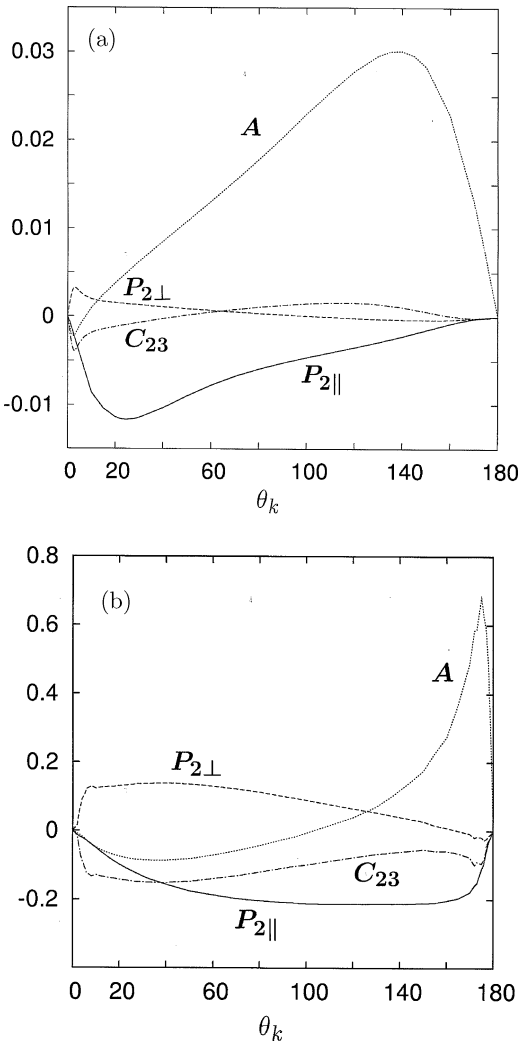

FIG. 6. Angular dependence of the polarization correlations $P_{2\parallel} = -C_{31}$ (solid curve), $P_{2\perp} = C_{11}$ (dashed curve), C_{23} (dot-dashed curve), and $A = C_{20}$ (dotted curve) from 10 MeV electrons colliding with Au^{79+}. (a) $\omega = 5$ MeV within the SM theory, (b) $\omega = 10$ MeV (SWL) within the DSM model.

In Fig. 6(a), the polarization correlations P_2, A, and C_{23} are displayed for $E_{i,\mathrm{kin}} = 10$ MeV and $\omega = 5$ MeV, using the Sommerfeld-Maue theory. It was derived by Tseng and Pratt [10] that $P_{2\perp} = -C_{23}$ near $\theta_k = 0$, and $P_{2\perp} = C_{23}$ near $\theta_k = 180^\circ$, which is clearly seen in the figure. However, as compared to the results for $\omega/E_{i,\mathrm{kin}} = 0.5$ at an impact energy of 0.5 MeV (Ref. [10], Fig. 26) the regime where $P_{2\perp}$ and C_{23} are approximately symmetric to each other extends to much larger angles ($\theta_k \lesssim 150^\circ$) with only a small region where the slopes of $P_{2\perp}$ and C_{23} roughly agree ($\theta_k \gtrsim 170^\circ$). The most striking feature when $E_{i,\mathrm{kin}}$ is increased from 0.5 to 10 MeV is the global decrease in modulus of the polarization correlations P_2 and C_{23} (up to one order of magnitude). Again, there is the relativistic focusing of the extrema to the forward angles. An exception is the spin asymmetry A, the maximum of which is shifted to backward angles and has a similar value at 0.5 and 10 MeV.

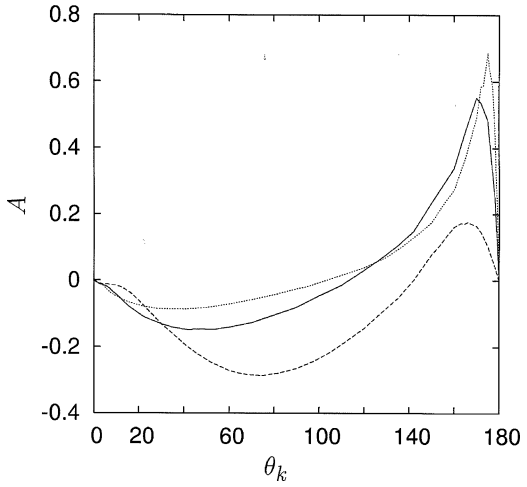

FIG. 7. Angular dependence of the spin asymmetry A from 2 MeV (dashed curve), 5 MeV (solid curve), and 10 MeV (dotted curve) electrons colliding with Au^{79+} at the SWL (DSM theory).

In Fig. 6(b), the same polarization correlations are plotted at the SWL, calculated within the DSM model. Since the emission of a 10 MeV photon requires very close collisions, relativity is extremely important, and the polarization correlations are indeed much larger than for $\omega = 5$ MeV. Both C_{23} and $P_{2\perp}$ exhibit a broad extremum in the forward hemisphere and an additional narrow minimum at angles close to 180°. As concerns the spin asymmetry A, it was predicted a long time ago, using a perturbative expansion, that A depends linearly on $Z\alpha$ [51]. In fact, at $\omega = 10$ MeV (and a gold target) the maximum of A is ~ 0.6 which is close to $Z\alpha = 0.58$. Moreover, as follows from Fig. 7, where the spin asymmetry at the SWL is shown for impact energies between 2 and 10 MeV, the maximum of A is still increasing with E_i in this energy regime (whereas the minimum in the forward hemisphere gets shallower). This increase of A up to at least $E_{i,\mathrm{kin}} = 10$ MeV is at variance with the conjecture of [51] that A should be largest for $v/c \approx 0.6$ (corresponding to $E_{i,\mathrm{kin}} \approx 130$ keV). It should be noted that there are no literature results for A at the SWL. However, even if we fix the ratio $\omega/E_{i,\mathrm{kin}} = 0.75$, then at 130 keV one has $|A| \lesssim 0.14$ at all photon angles [10], whereas the SM calculations at $E_{i,\mathrm{kin}} = 10$ MeV (and the same ratio) predict $A \approx 0.17$ in its maximum near $\theta_k = 140°$.

VI. CONCLUSION

We have investigated the photon angular distribution and the polarization correlations resulting from bremsstrahlung of highly relativistic spin-polarized electrons colliding with heavy ions such as gold. Particular emphasis was laid on the short-wavelength limit where the electron transfers all its kinetic energy to the photon. For this process the DSM theory was developed where the wave function of the incoming electron is described by a Sommerfeld-Maue function in place of an exact relativistic function. This approximation, valid above 5 MeV impact energy (except possibly at the largest photon angles), leads to a considerable reduction of computer time as compared to the relativistic partial-wave calculations, thus allowing collision energies up to at least 10 MeV. The DSM model can readily be extended to a small region below the SWL by replacing the Bessel functions in (2.6) by the corresponding exact radial functions and by including some more final-state partial waves. The basic advantage of this model, the small number of partial waves, is, however, lost when photons with an energy much lower than the SWL are considered.

Our main concern was the improvement of the doubly differential cross section at the SWL as compared to the results from the commonly used Elwert-Haug theory. Indeed, for the two test cases $E_{i,\mathrm{kin}} = 180$ and 380 keV where experimental data and partial-wave results are available, the DSM model performs well except for photon angles above 130°. This region of validity shrinks to smaller angles when the collision energy is increased to 2 MeV. Only beyond 5 MeV will the Sommerfeld-Maue function again perform well as conjectured from the results of [38].

We have also studied the dependence of the polarization correlations on photon energy and angle at 10 MeV and have compared our results with the corresponding results of Tseng and Pratt at 0.5 MeV, the highest collision energy considered by these authors for a heavy (gold) target. For P_1 we observe, similar to the elementary process of bremsstrahlung (i.e., when electrons and photons are detected simultaneously in a coplanar geometry [52]), that P_1 is closest to unity when the differential cross section has its maximum. The forward focusing at 10 MeV is also seen for P_2 and C_{23}.

An exception is the spin asymmetry A which gets strongly focused near $\theta_k = 180°$ when the collision energy is increased. While the other polarization correlations are subject to an overall decrease of modulus with collision energy beyond 2 MeV, the maximum of A increases with $E_{i,\mathrm{kin}}$, at least up to 10 MeV. At collision energies near 15 MeV and θ_k near 180° the relevant distances will reach $r = 1.3 \times 10^{-4}$a.u. $= 7$ fm, which is the radius of the Au nucleus. Thus A is a candidate for measuring nuclear size effects when $E_{i,\mathrm{kin}} > 10$ MeV (see the predictions of [53] for the elastic backscattering of spin-polarized electrons).

ACKNOWLEDGMENTS

It is a pleasure to thank S. Tashenov for stimulating this project, and A. Surzhykov for valuable comments and for providing new partial-wave results. I am also indebted to R. Pratt for many helpful remarks.

[1] J. Eichler and Th. Stöhlker, Phys. Rep. **439**, 1 (2007).
[2] Th. Stöhlker *et al.*, Phys. Rev. Lett. **86**, 983 (2001).
[3] M. Nofal *et al.*, Phys. Rev. Lett. **99**, 163201 (2007).
[4] V. V. Balashov, A. N. Grum-Grzhimailo, and N. M. Kabachnik, *Polarization and Correlation Phenomena in Atomic Collisions* (Kluwer Academic/Plenum, New York, 2000).

[5] A. Surzhykov, S. Fritzsche, Th. Stöhlker, and S. Tashenov, Phys. Rev. A **68**, 022710 (2003).
[6] S. Tashenov *et al.*, Phys. Rev. Lett. **97**, 223202 (2006).
[7] H. Olsen and L. C. Maximon, Phys. Rev. **114**, 887 (1959).
[8] H. Brysk, C. D. Zerby, and S. K. Penny, Phys. Rev. **180**, 104 (1969).
[9] E. Haug, Phys. Rev. **188**, 63 (1969).
[10] H. K. Tseng and R. H. Pratt, Phys. Rev. A **7**, 1502 (1973).
[11] J. W. Motz and R. C. Placious, Nuovo Cimento **15**, 571 (1960).
[12] M. Scheer, E. Trott, and G. Zahs, Z. Phys. **209**, 68 (1968).
[13] R. W. Kuckuck and P. J. Ebert, Phys. Rev. A **7**, 456 (1973).
[14] K. Güthner, Z. Phys. **182**, 278 (1965).
[15] A. Aehlig, Z. Phys. A **294**, 291 (1980).
[16] E. Mergl and W. Nakel, Z. Phys. D **17**, 271 (1990).
[17] E. Mergl, H.-Th. Prinz, C. D. Schröter, and W. Nakel, Phys. Rev. Lett. **69**, 901 (1992).
[18] E. Haug, Z. Phys. D **37**, 9 (1996).
[19] C. D. Shaffer, X.-M. Tong, and R. H. Pratt, Phys. Rev. A **53**, 4158 (1996).
[20] S. Tashenov *et al.* (unpublished).
[21] R. Märtin *et al.*, contributed paper to CAARI, Denton, Texas, 2010 (unpublished).
[22] R. Barday (private communication); in WSPC Proceedings, 2009 (unpublished).
[23] H. A. Bethe and L. C. Maximon, Phys. Rev. **93**, 768 (1954).
[24] G. Elwert and E. Haug, Phys. Rev. **183**, 90 (1969).
[25] A. Sommerfeld and A. W. Maue, Ann. Physik **22**, 629 (1935).
[26] V. B. Berestetskii, E. M. Lifshitz, and L. P. Pitaevskii, *Quantum Electrodynamics*, Course of Theoretical Physics Vol. 4 (Elsevier, Oxford, 1982), Chap. 39.
[27] J. D. Rozics and W. R. Johnson, Phys. Rev. **135**, B56 (1964).
[28] H. K. Tseng and R. H. Pratt, Phys. Rev. A **3**, 100 (1971).
[29] R. H. Pratt, H. K. Tseng, C. M. Lee, L. Kissel, C. MacCallum, and M. Riley, At. Data Nucl. Data Tables **20**, 175 (1977); **26**, 477 (1981).
[30] H. K. Tseng and R. H. Pratt, Phys. Rev. A **19**, 1525 (1979).
[31] E. Haug, Eur. Phys. J. D **58**, 297 (2010).
[32] R. J. Jabbur and R. H. Pratt, Phys. Rev. **129**, 184 (1963); **133**, B1090 (1964).
[33] R. H. Pratt and H. K. Tseng, Phys. Rev. A **11**, 1797 (1975).
[34] I. J. Feng, I. B. Goldberg, Y. S. Kim, and R. H. Pratt, Phys. Rev. A **28**, 609 (1983).
[35] A. Burgess and M. Seaton, Rev. Mod. Phys. **30**, 992 (1958).
[36] C. M. Lee and R. H. Pratt, Phys. Rev. A **12**, 1825 (1975).
[37] A. Surzhykov (private communication).
[38] D. H. Jakubassa-Amundsen and A. Surzhykov (unpublished).
[39] W. Heitler, *The Quantum Theory of Radiation*, 3rd ed. (Oxford University, New York, 1954), Chap. 25.
[40] D. H. Jakubassa-Amundsen, J. Phys. B **40**, 2719 (2007).
[41] E. M. Rose, *Relativistic Electron Theory* (Wiley, New York, 1961), Chaps. 15, 19, 33.
[42] A. R. Edmonds, *Angular Momentum in Quantum Mechanics* (Princeton University, Princeton, NJ, 1964) Secs. 2.5, 5.9.
[43] V. S. Popov, Sov. J. Nucl. Phys. **12**, 235 (1971).
[44] I. S. Gradshteyn and I. M. Ryzhik, *Table of Integrals, Series and Products* (Academic, New York, 1965).
[45] R. Estrada and R. P. Kanwal, *A Distributional Approach to Asymptotics: Theory and Applications* (Birkhäuser, Boston, 2002), Chap. 6.10.
[46] C. J. Joachain, *Quantum Collision Theory* (North-Holland, Amsterdam, 1987), Chap. 5.2.
[47] M. Kleber and D. H. Jakubassa, Nucl. Phys. A **252**, 152 (1975).
[48] G. Weber, Ph.D thesis, University of Heidelberg, 2010.
[49] O. Forster, *Analysis I*, 9th ed. (Vieweg, Wiesbaden, 2008), Chap. 20.
[50] H. Aiginger, Z. Phys. **197**, 8 (1966).
[51] W. R. Johnson and J. D. Rozics, Phys. Rev. **128**, 192 (1962).
[52] W. Nakel, Rad. Phys. Chem. **75**, 1164 (2006).
[53] P. Uginčius, H. Überall, and G. H. Rawitscher, Nucl. Phys. A **158**, 418 (1970).